

SANDIA REPORT

SAND2006-7081

Unlimited Release

Printed November 2006

Membranes for H₂ Generation from Nuclear Powered Thermochemical Cycles

Tina M. Nenoff, Andrea Ambrosini, Terry J. Garino, Kevin Leung, Marlene Axness, Fred Gelbard, Ratnasabapathy G. Iyer, Alexandra Navrotsky

Prepared by
Sandia National Laboratories
Albuquerque, New Mexico 87185 and Livermore, California 94550

Sandia is a multiprogram laboratory operated by Sandia Corporation, a Lockheed Martin Company, for the United States Department of Energy's National Nuclear Security Administration under Contract DE-AC04-94AL85000.

Approved for public release; further dissemination unlimited.

Issued by Sandia National Laboratories, operated for the United States Department of Energy by Sandia Corporation.

NOTICE: This report was prepared as an account of work sponsored by an agency of the United States Government. Neither the United States Government, nor any agency thereof, nor any of their employees, nor any of their contractors, subcontractors, or their employees, make any warranty, express or implied, or assume any legal liability or responsibility for the accuracy, completeness, or usefulness of any information, apparatus, product, or process disclosed, or represent that its use would not infringe privately owned rights. Reference herein to any specific commercial product, process, or service by trade name, trademark, manufacturer, or otherwise, does not necessarily constitute or imply its endorsement, recommendation, or favoring by the United States Government, any agency thereof, or any of their contractors or subcontractors. The views and opinions expressed herein do not necessarily state or reflect those of the United States Government, any agency thereof, or any of their contractors.

Printed in the United States of America. This report has been reproduced directly from the best available copy.

Available to DOE and DOE contractors from
U.S. Department of Energy
Office of Scientific and Technical Information
P.O. Box 62
Oak Ridge, TN 37831

Telephone: (865) 576-8401
Facsimile: (865) 576-5728
E-Mail: reports@adonis.osti.gov
Online ordering: <http://www.osti.gov/bridge>

Available to the public from
U.S. Department of Commerce
National Technical Information Service
5285 Port Royal Rd.
Springfield, VA 22161

Telephone: (800) 553-6847
Facsimile: (703) 605-6900
E-Mail: orders@ntis.fedworld.gov
Online order: <http://www.ntis.gov/help/ordermethods.asp?loc=7-4-0#online>



Membranes for H₂ Generation from Nuclear Powered Thermochemical Cycles

Tina M. Nenoff, Andrea Ambrosini, Terry Garino, Kevin Leung, Marlene Axness, Fred Gelbard, Ratnasabapathy G. Iyer[#], Alexandra Navrotsky[#]

Sandia National Laboratories,
PO Box 5800,
Albuquerque, NM, 87185

[#]Department of Chemical Engineering and Material Science,
University of California,
Davis, CA 95616

ABSTRACT

In an effort to produce hydrogen without the unwanted greenhouse gas byproducts, high-temperature thermochemical cycles driven by heat from solar energy or next-generation nuclear power plants are being explored. The process being developed is the thermochemical production of Hydrogen. The Sulfur-Iodide (SI) cycle was deemed to be one of the most promising cycles to explore. The first step of the SI cycle involves the decomposition of H₂SO₄ into O₂, SO₂, and H₂O at temperatures around 850 °C. *In-situ* removal of O₂ from this reaction pushes the equilibrium towards dissociation, thus increasing the overall efficiency of the decomposition reaction. A membrane is required for this oxygen separation step that is capable of withstanding the high temperatures and corrosive conditions inherent in this process. Mixed ionic-electronic perovskites and perovskite-related structures are potential materials for oxygen separation membranes owing to their robustness, ability to form dense ceramics, capacity to stabilize oxygen nonstoichiometry, and mixed ionic/electronic conductivity. Two oxide families with promising results were studied: the double-substituted perovskite A_xSr_{1-x}Co_{1-y}B_yO_{3-δ} (A=La, Y; B=Cr-Ni), in particular the family La_xSr_{1-x}Co_{1-y}Mn_yO_{3-δ} (LSCM), and doped La₂Ni_{1-x}M_xO₄ (M = Cu, Zn). Materials and membranes were synthesized by solid state methods and characterized by X-ray and neutron diffraction, SEM, thermal analyses, calorimetry and conductivity. Furthermore, we were able to leverage our program with a DOE/NE sponsored H₂SO₄ decomposition reactor study (at Sandia), in which our membranes were tested in the actual H₂SO₄ decomposition step.

TABLE OF CONTENTS

Section	Page
Introduction.....	7
Experimental Section.....	7
Characterization.....	7
Results and Discussion.....	9
Conclusion.....	13
Acknowledgements.....	14
References.....	15
Figure Captions.....	17
Table 1.....	18
Figure 1.....	19
Figure 2.....	20
Figure 3.....	21
Figure 4.....	22
Figure 5.....	22
Table 2.....	23
Figure 6.....	24
Figure 7.....	25
Figure 8.....	25
Figure 9.....	26
Figure 10.....	26

INTRODUCTION

Efficient and environmentally friendly methods for producing hydrogen are important as the world explores the use of hydrogen as a clean energy source. One such method is the production of hydrogen via high-temperature thermochemical cycles driven by heat from solar energy or next-generation nuclear power plants.[1] These processes are advantageous because they do not produce greenhouse gas emissions that result from hydrogen production by electrolysis (using fossil fuel electricity sources) or hydrocarbon reformation. Based on a previous extensive survey of over 100 thermochemical cycles, which evaluated metrics such as efficiency, cost, number of steps, and the number and phases of reactants, the Sulfur-Iodide (SI) cycle was deemed to be one of the most promising.[2-4] The first step of the SI cycle involves the decomposition of H_2SO_4 into O_2 , SO_2 , and H_2O at temperatures around 850 °C. *In-situ* removal of O_2 from this reaction pushes the equilibrium towards dissociation, thus increasing the overall efficiency of the decomposition reaction. The membrane required for this oxygen separation step must withstand the high temperatures and corrosive conditions inherent in this process.

Perovskites and perovskite-related structures are potential materials for oxygen separation membranes owing to their robustness, ability to form dense ceramics, capacity to stabilize oxygen nonstoichiometry, and mixed ionic/electronic conductivity.[5-9] A mixed ionic-electronic conductor benefits the process by allowing the separation of oxygen via ionic conductivity, while the electronic conductivity eliminates the need for an applied potential across the membrane to balance the oxygen ion flux. To this end, a survey (literature and experimental) of potential perovskite and related compounds was undertaken. Powder samples were synthesized by solid state methods and characterized using powder X-ray diffraction (XRD), thermogravimetric analysis (TGA), and elemental analysis. TGA versus temperature and oxygen partial pressure was used as a screening method to test the oxygen absorption and desorption properties and stability of the materials. Two oxide families with promising initial results were decided upon for further study: the double-substituted perovskite $\text{La}_x\text{Sr}_{1-x}\text{Co}_{1-y}\text{Mn}_y\text{O}_{3-\delta}$ (LSCM) and doped La_2NiO_4 .

EXPERIMENTAL SECTION

Synthesis. For the LSCM class of materials: the oxides were synthesized by the Pechini method to ensure more complete mixing of the reactants.[10] Stoichiometric amounts (metals basis) of metal nitrates were dissolved in deionized H_2O . Citric acid was added in a 1.5:1 citric acid:metal molar ratio and the solution was heated to 90 °C with stirring until a gel formed. The gel was dried overnight at 100 °C and then ignited at 350-400 °C to burn off the nitrates and citrates. The resulting powder was ground with an agate mortar and pestle, calcined at 950 °C for 24 hours, re-ground, and sintered again at 1250 °C for 24-96 hours.

For the $\text{La}_2\text{Ni}_{1-x}\text{M}_x\text{O}_4$ ($\text{M} = \text{Cu}, \text{Zn}$) class of materials: phases were synthesized via solid state synthesis method. Stoichiometric amounts of oxides were ground together and sintered in a crucible at 1000°C for 24 hours, then ground again and resintered at 1250°C for 24 hours.

CHARACTERIZATION

Permeation. Circular, 12 mm-diameter self-supported membranes of LSCM were synthesized by isostatic pressing and sintering of the powders and characterized by X-ray diffraction, four-probe conductivity, and scanning electron microscopy. A high-temperature oxygen permeation unit was constructed for oxygen permeability measurements up to 900 °C,

and additional permeation measurements on the LSCM materials were taken in collaboration with Eltron Research, Inc. In addition, the materials were placed in a H₂SO₄ decomposition reactor, designed and operated by Fred Gelbard, to test for stability under high temperature and corrosive conditions.

Structural characterization. The material structure was characterized by powder x-ray diffraction (PXRD) on a Siemens D500 diffractometer (Cu K_α radiation, Bragg-Brentano geometry) and refined using the Jade 6.5+ [11] and FullProf [12] Rietveld or GSAS refinement software. Structures were also refined, and impurity peaks sought, in samples used for calorimetry at UC Davis using a Scintag PAD-V diffractometer and Jade 6.5+ [11] software.

Thermal studies. Thermal studies on powder samples were performed using a TA Instruments STD 2960 DTA-TGA; the data were used to obtain information about structural stability and oxygen absorption/desorption. For absorption/desorption studies, multiple-cycle thermogravimetric analysis (TGA) was run. First the temperature was cycled between 50 - 850°C under an O₂ atmosphere. This was followed by cycling between O₂ (high pO₂) and Ar or He (low pO₂) atmospheres at 850°C. The flow rate of the gases was approximately 130 sccm. PXRD studies were run before and after thermal study samples to confirm that the material retained its original perovskite structure.

Conductivity Measurements. The sintered samples were cut using a diamond saw into bars nominally 1 x 0.2 x 0.2 cm. Four Pt wires were wrapped around each bar and bonded to the sample using Ag-Pd paste (ESL 963, 20% Pd, Electro Sciences Labs, PA, USA). The samples were heated to 950 °C to sinter the conducting paste. The conductivity measurements were performed in a tube furnace with an alumina tube using Pt wires to connect the wires on the sample in the hot zone. These wires were then fed through the end cap of the tube which also had gas inlet and outlet ports to allow control of the atmosphere. Four-point DC electrical conductivity measurements were performed by sending a current (0.01 to 100 mA) through the wires at the ends of the sample and then measuring the voltage drop across and two middle wires. The furnace was allowed to equilibrate at each measurement temperature for about 1 hour. The oxygen partial pressure in the atmosphere was controlled by using compressed gases (O₂, UHP Ar, and O₂/Ar mixtures) and was measured after it passed through the furnace using a pO₂ meter. After a change in atmosphere, the sample was allowed to equilibrate until the measured voltage was constant, typically about 1 hour. The conductivity was calculated from the applied current, the measured voltage and the sample dimensions.

Calorimetry. High temperature reaction calorimetry refers to the measurement of heats of chemical reactions at temperatures above approximately 400 °C. The calorimeters used are of several types, but most have several features in common. They generally measure heat flow between a sample and heat sink maintained at an essentially constant temperature; thus they are of isoperibol type. A twinned Calvet microcalorimeter is used in the UC Davis Thermochemistry Facility, with two sample chambers; each surrounded by a Pt-PtRh thermopile linking it to a constant temperature metallic block (Inconel alloy). The thermopiles are linked in series opposition, and the twinned design both increases productivity and, more importantly, helps minimize the deleterious effects of small drifts in the furnace and/or ambient temperature. Control of ambient temperature, humidity, and airflow is required to obtain good signal stability (baseline). 5-15 mg samples are used; the solvent is typically 2PbO·B₂O₃ or 3Na₂O·4MoO₃.

Modeling. Density functional theory (DFT) calculations were performed for the end member material SrCoO₃, SrFeO₃, and La_{0.125}Sr_{0.875}Co_{0.875}Mn_{0.125}O_{3-δ} and La_{0.125}Sr_{0.875}Co_{0.875}Fe_{0.125}O_{3-δ}. We used supercells (i.e., replications of the basic formula unit cubic primitive

cell) of size 2x2x2, containing 40 atoms; $\delta=0$ or 0.042, corresponding to +/- one oxygen vacancy. We applied the VASP code, a 400 eV energy cut off, and k-point grids of density up to 3x3x3 for this supercell (equivalent to a 6x6x6 grid for the 5 atom primitive unit cell). Both the GGA and DFT+U methods were used in these calculations.

Permeation Units. An in-house permeation unit was built at Sandia. The permeation unit was designed to operate at temperatures up to 900 °C at pressures at or below 2 atm. Commercially available stainless steel Swagelok components, stainless steel tubing, and copper tubing designed for pressurized applications were used in the construction of the unheated portions of the permeation unit. Inconel 600 tubing (Ni metal alloy) was used for the portion that operates at high temperature. The permeation unit is heated by placing it in a 1” diameter Lindberg tube furnace with a programmable temperature controller. Flow is controlled by installed Brooks 5050E series mass flow controllers. Air (79% N₂ : 21% O₂ mixture) is flowed into one end of the unit, while a He carrier gas flows through the other end, separated by a dense ceramic membrane. The membrane is sealed onto the permeation unit using Cermet Ag ink 9990 (Electro-Science Labs, Inc). Both gases exit through outlet ports and the overall pressure within the unit does not exceed 2 atm. The He outlet is plumbed into a micro gas chromatograph (Agilent) in order to identify the retentate gases, which are expected to be He and O₂. The presence of N₂ in the retentate is indicative of a leak.

Additional testing of the membrane materials occurred in a H₂SO₄ decomposition reactor built by Fred Gelbard. [For details of general reactor set-up, see reference 13.] These experiments were used to test the stability of the materials under reactor conditions of H₂SO₄ decomposition.

RESULTS AND DISCUSSION

While a number of B-type cations were substituted into the La_{0.1}Sr_{0.9}Co_{1-y}B_yO_{3- δ} material (B = Cr, Mn, Fe, Ni, Cu), the most promising phases in this study to date, based on structure and sorption properties, are in the Mn-substituted (LSCM) family. The compositions of the Mn-synthesized materials, their purity, lattice parameters, and average weight loss versus temperature and oxygen partial pressure are listed in Table 1a. Ytria-stabilized zirconia (YSZ), a well-known ion conductor, is included for comparison purposes.

The double-substituted perovskites were indexed in the cubic *Pm-3m* (221) space group; the Rietveld refinement of an LSCM sample is shown in Figure 1. The PXRD patterns of a series of LSCM materials, La_{0.1}Sr_{0.9}Co_{1-y}Mn_yO_{3- δ} (0.1 ≤ y ≤ 0.5), are shown in Figure 2. The material is single phase up to y = 0.3, then a secondary phase (as yet unidentified) begins to form. Although Petrov *et al.* report a complete solid solution for La_{0.7}Sr_{0.3}Co_{1-y}Mn_yO_{3- δ} , the materials were synthesized under different conditions and crystallized in the rhombohedral space group, *R-3c*. [14] The cubic lattice parameter decreases in the single phase materials as the concentration of Mn increases. Increasing the La:Sr ratio appears to stabilize increased concentrations of Mn, i.e., while LSCM1955 is multi-phase, LSCM5555 is single phase. However, as seen in Table 1a, increasing the concentration of La generally results in a decrease in oxygen sorption versus pO₂.

Figure 3a illustrates an example of a multiple-cycle TGA analysis of an LSCM1973. It has been shown that such TGA analysis is an effective screening method for potential oxygen permeability. [15,16] The first part of the graph shows the weight change as the temperature is cycled between 50-850 °C, under a flow of O₂ gas. A weight change demonstrates a reversible temperature-swing adsorption/desorption of oxygen. The second part of the graph illustrates the reversible weight change as a function of oxygen partial pressure, by cycling the gas between O₂ and Ar or He at 850 °C. This implies that the material can transport oxygen across a membrane

with an oxygen partial pressure differential. An analogous TGA cycle of the ionic conductor YSZ is shown in Fig. 3b; the magnitude of oxygen sorption in YSZ is much less than that of any LSCM material. For comparison purposes, multi-cycle TGA was also performed on samples of $\text{La}_{0.1}\text{Sr}_{0.9}\text{Co}_{0.9}\text{Fe}_{0.1}\text{O}_{3-\delta}$ and $\text{La}_{0.1}\text{Sr}_{0.9}\text{CoO}_{3-\delta}$, both of which are oxygen separation materials, as reported in the literature, and have similar compositions to the LSCM materials reported herein.[5,15,17] These compounds were synthesized by the same method as the LSCM materials, and the TGA conditions were analogous so as to allow direct comparison. The results are shown in Table 1a; the $\text{La}_{0.1}\text{Sr}_{0.9}\text{Co}_{1-y}\text{Mn}_y\text{O}_{3-\delta}$ ($0.1 \leq y \leq 0.3$) materials compare favorably with the values of these known permeation materials. In general, the sorption properties versus $p\text{O}_2$ for the LSCM materials increase with increasing concentrations of Mn and decreasing La, until the solid solubility of Mn in the structure is reached.

PXRD performed on post-TGA samples reveals that no structural changes occur as a result of the temperature and gas treatments, demonstrating the robustness of the material. A sample of LSCM1973 was cooled under Ar gas in order to maintain the oxygen deficiency in the material and determine that no phase transition occurs under reducing conditions. PXRD of this sample and the lack of exothermic/endothemic peaks in the DTA of any of the LSCM samples support the conclusion that no phase change occurs in the sample during the TGA cycle

Conductivity measurements were performed on promising LSCM samples, as well as on a standard YSZ sample. Figure 4a shows the plot of conductivity versus temperature in air, while Figure 4b shows the dependence of conductivity versus $p\text{O}_2$. In both cases, the overall conductivity of the LSCM is more than three orders of magnitude greater than that of YSZ. Such a high conductivity implies a high degree of electronic (as opposed to ionic) conductivity. Ionic conductivity is present as well, based on preliminary ionic conductivity measurements, but it is overshadowed by the electronic character.[5,18] As seen in Figure 4a, the conductivity of LSCM slightly increases with temperature, implying that it is a semiconductor. The material properties are also dependent on $p\text{O}_2$, as its conductivity decreases slightly with decreasing $p\text{O}_2$, indicating an overall p-type character. This behavior is similar to that reported for other members of the LSCM family.[18]

Another class of materials we studied was substituted La_2NiO_4 , in which Zn and Cu were substituted into the material. [19] The compositions of the $\text{La}_2\text{Ni}_{1-x}\text{M}_x\text{O}_4$ synthesized materials, their purity, lattice parameters, and average weight loss versus temperature and oxygen partial pressure are listed in Table 1b.

Thermal cycling studies were also conducted on the $\text{La}_2\text{Ni}_{1-x}\text{M}_x\text{O}_4$ materials, in the same manner described above for the LSCM samples. Results (as seen in table 1b) indicate that both pure and substituted samples had noticeable weight loss versus temperature. The substituted compositions showed the largest weight loss versus $p\text{O}_2$. These indicated that these materials were viable candidates for our oxygen separation membranes.

Conductivity measurements of $\text{La}_2\text{Ni}_{1-x}\text{M}_x\text{O}_4$ materials were the next set of experiments to determine viability as membrane materials. The samples tested were La_2NiO_4 , $\text{La}_2\text{Ni}_{0.8}\text{Zn}_{0.2}\text{O}_4$ and $\text{La}_2\text{Ni}_{0.6}\text{Zn}_{0.4}\text{O}_4$; the procedure was the same as that described above. The conductivity testing showed results (as seen in figure 5) on the same order of magnitude as the LSCM materials, with consistently higher conductivity for the unsubstituted material (La_2NiO_4). (Ionic Radii: Zn^{2+} (VI) = 0.74 Å, Cu^{2+} (VI) = 0.73 Å, Ni^{2+} (VI) = 0.69 Å). [20] Further research is needed to elucidate the phenomena resulting in the change in conductivity.

Calorimetry. The thermochemical cycle was completed for LSCM materials along with the table containing the enthalpies of formation from oxides and elements (see table 2). Further analysis of the LSCM samples and the cobalt end member $\text{La}_{0.1}\text{Sr}_{0.9}\text{CoO}_3$ (LSC 191) was completed, see figure 6. Iodometric titration of LSC 191 gave an average delta value (oxygen deficient) of 0.29 ± 0.01 . Based on the microprobe analysis of the sample, a composition was determined to be $\text{La}_{0.1}\text{Sr}_{0.96}\text{Co}_{1.07}\text{O}_{2.72}$, that $\text{La}_{0.1}\text{Sr}_{0.96}\text{Co}_{1.07}\text{O}_{2.72}$, which is consistent with the observed oxygen content and a charge of 3+ for Co. In order to find a trend in the observed enthalpies of formation from oxides for the three LSCM compositions, an average oxidation state (AOS) of Mn for 10 ratios of $[\text{Co}^{3+}/(\text{Co}^{3+} + \text{Co}^{4+})]$ was calculated. It was observed that for a ratio of 0.6 (this ratio is unique), there is an almost linear correspondence in the AOS of Mn with respect to the enthalpies of formation. This is shown in the following table:

LSCM	AOS of Mn	ΔH_{ox}^{0f} kJ/mol
$\text{La}_{0.1}\text{Sr}_{0.9}\text{Co}^{3+}_{0.48}\text{Co}^{4+}_{0.32}\text{Mn}_{0.2}\text{O}_{2.76}$	3.5	-105.43 ± 2.27
$\text{La}_{0.1}\text{Sr}_{0.9}\text{Co}^{3+}_{0.54}\text{Co}^{4+}_{0.36}\text{Mn}_{0.1}\text{O}_{2.76}$	3.6	-113.52 ± 2.28
$\text{La}_{0.1}\text{Sr}_{0.9}\text{Co}^{3+}_{0.39}\text{Co}^{4+}_{0.26}\text{Mn}_{0.35}\text{O}_{2.8}$	3.69	-115.60 ± 2.28
$\text{La}_{0.1}\text{Sr}_{0.9}\text{Co}^{3+}_{1.07}\text{O}_{2.72}$	0	-142.36 ± 2.61

Density functional theory modeling.

An extensive review of the theoretical and experimental literature on the phase diagram of the quaternary system (La/Sr)(Co/Mn)O₃ perovskites was made to provide insight into the DFT modeling and help ascertain the accuracy of the theoretical methods used. Due to the strong electron correlation in the first row transition metal ions, this class of perovskites exhibits rich and complex structural, electronic, and magnetic behavior. (1) The end member SrCoO₃ is known to be metallic [21], with a 2.1 Bohr magneton magnetic moment per formula unit. LDA calculations qualitatively reproduce these properties [22]. (2) Another end member, LaCoO₃, is diamagnetic and an insulator at zero temperature [23]. LDA calculations erroneously predict metallic behavior; in contrast, the DFT+U method, which takes into account static correlations among the strongly localized metal 3d electrons, successfully predicts a finite band gap [24]. (3) Depending on the composition x, the solid solution $\text{La}_x\text{Sr}_{1-x}\text{MnO}_3$ exhibits colossal magnetoresistance and temperature-dependent metal-insulator transitions [25]. Oxygen vacancies and the possible existence of multiple crystallographic phases (cubic, rhombohedral, hexagonal) further complicate the analysis. LDA results for these Mn-based perovskites appear adequate [26].

With this range of behavior in mind, we first performed GGA and DFT+U calculations for SrCoO₃. (GGA and LDA results are similar; we adopt the former for historical reasons.) The two methods predict magnetic moments of 2.5 and 3.3 Bohr magneton, respectively. The experimental result is 2.1, indicating that GGA is more accurate. This is consistent with published results for NaCoO₂; in that metallic material, LDA is more accurate than DFT+U as well [27], and the failure of DFT+U was attributed to its inability to treat dynamical electron correlations in metallic systems.

Thus, while there is no theoretical (electronic structure) method that is universally applicable across the very complex LSCM quaternary phase diagram, experimental data and our calculations on the end members suggest the following trend. (1) When DFT+U predicts a finite

band gap, and GGA does not, the DFT+U method is more accurate. (2) When GGA and DFT+U both predict a zero band gap, the material is a metal, and GGA is likely the more reliable method.

Armed with this criterion, we consider 12.5% doped LCSM ($\text{La}_{0.125}\text{Sr}_{0.875}\text{Co}_{0.875}\text{Mn}_{0.125}\text{O}_{3-\delta}$, i.e., one La and one Mn atom per $2\times 2\times 2$ supercell containing 40 atoms). Just like the case of SrCoO_3 , both methods predict zero band gaps and ferromagnetic behavior. From the above discussion, we tentatively concluded that this composition of LCSM exhibits a zero band gap, and GGA should be the method of choice. Note that comparison with our conductivity experiments, which appeared to reveal semiconducting behavior, is complicated by the amount of oxygen vacancy in the system. At present, the electronic properties of these oxides remain unresolved; more conclusive theoretical methods need to be developed.

Next, we considered $\text{La}_{0.125}\text{Sr}_{0.875}\text{Co}_{0.875}\text{Mn}_{0.125}\text{O}_{3-\delta}$, with one oxygen vacancy in the $2\times 2\times 2$ supercell. GGA predicts a zero band gap. Using a method we published previously, the oxygen vacancy hopping barrier was found to be small, on the order of 0.30 eV. This is much smaller than the barrier in natural occurring perovskites such as potassium tantalite [28]. The low energy barrier for oxygen motion through vacancies translates into fast oxygen transport, and suggests that LSCM is indeed specially suited as an oxygen permeable membrane.

Finally, we examined LSCF, where Fe replaced Mn on the perovskite B-site. The electronic and magnetic properties of $\text{La}_{0.125}\text{Sr}_{0.875}\text{Co}_{0.875}\text{Fe}_{0.125}\text{O}_{3-\delta}$ were found to be similar those of LSCM of the same composition, while the oxygen vacancy hopping barrier was found to be 0.58 eV. This is substantially higher than that for LSCM, supporting the idea LSCM represents a more promising candidate as oxygen transport membrane.

H₂SO₄ Decomposition Reactor.

A pellet of LSCM1973 was placed in the pressurized acid decomposition reactor in order to test the stability of the material under operating conditions. The reactor was run at 850 °C under approximately 1.5 atm of pressure. Several runs were made on the reactor before the membrane was removed, and it is not known if the membranes were exposed to residual, condensed H₂SO₄. The sample was removed intact, *i.e.* it did not decompose completely during the reactor runs.

PXRD was performed on the both the surface of the pellet and a crushed-up piece of the pellet in order to get an idea of the overall level of corrosion. Figure 7 shows the diffraction patterns of the pellet both before and after exposure to the H₂SO₄ decomposition stream. The results were mixed. The crushed-up LSCM powder seemed to have remained largely single-phase, with only small peaks corresponding to SrSO₄. Diffraction of the surface, however, shows a larger concentration of corrosion products, specifically SrSO₄, but also possible traces of decomposition products such as MnO, Mn and Co₃O₄.

The next step was to determine the extent of the corrosion of the pellet, which was achieved by SEM of the surface and cross-section of the pellet by Bonnie McKenzie at Sandia National Laboratories. Figure 8 shows SEM of the surface of the pellet before and after the decomposition reaction. Some corrosion is visible. EDS confirms the presence of sulfur on the surface. Following surface analysis, a cross section of the pellet was prepared by fast-ion beam (Figure 9) and analyzed by SEM and EDS. Figure 9 shows the cross-section and the EDS maps for Co, Sr (major components of the pellet material) and S. A layer containing sulfur exists for approximately 2-4 microns, but was not observed in the rest of the pellet.

Permeation Results.

Mixed conducting membranes prepared at Sandia were tested for oxygen permeation and ionic conductivity at Eltron Research, Inc.; permeation testing at Sandia was not successful. Eltron's results are reported in full in their final report (March 9, 2006). [29] Three samples of LSCM (1973, 1982, and 1991) were tested between 800° and 950°C. All samples showed signs of some leaking, which was corrected for. Permeation results of the three compositions show high oxygen permeation. Doping of manganese into the $\text{La}_{0.1}\text{Sr}_{0.9}\text{CoO}_3$ structure results in materials which, under relatively mild conditions, still exhibit permeation rates in excess of $1 \text{ ml}/\text{min}\cdot\text{cm}^2$ at lower doping levels. One would expect a regular trend in permeation as a function of composition. These results do not show that trend. (See figure 10.) Eltron's researchers believe that the reason for this may be the higher leak observed in the 1982 sample, resulting in what might be anomalously high permeation numbers. The activation energy does show a regular increase with increase in Mn content.

Based on the good wetting observed of the Pyrex o-ring seal with the membrane, Eltron researchers believe the leaks result from defects and/or porosity in the membranes. Materials of similar composition exhibit very high expansion. In order to fabricate membranes with minimum defects, Eltron controls powder particle size, adds appropriate binders to increase green density, adjusts sintering temperature to avoid over sintering, and adjusts temperature ramp rates in sintering to avoid thermal shock to disk.

Further work is ongoing to form and test the LSCM materials as densified disk membranes to avoid microcracking and gas leakages.

CONCLUSION

Double-substituted perovskites with the formula $\text{La}_{0.1}\text{Sr}_{0.9}\text{Co}_{1-y}\text{B}_y\text{O}_{3-\delta}$ (B=Fe, Ni, Cr, Mn), as well as $\text{La}_2\text{Ni}_{1-x}\text{M}_x\text{O}_4$ (M = Cu, Zn) were synthesized for use as ceramic high-temperature oxygen separation membranes for the thermochemical production of hydrogen and other potential high temperature applications. The most promising materials from our study belong to the family of $\text{La}_{0.1}\text{Sr}_{0.9}\text{Co}_{1-y}\text{B}_y\text{O}_{3-\delta}$ where B = Mn. [30] Results indicate these materials have promising oxygen sorption properties and are structurally robust under varying temperatures and atmospheres. Four-probe conductivity measurements of the LSCM show semiconducting behavior. Continuing work is underway, testing the LSCM materials as membranes for permeation experiments and material stability under "real time" reaction conditions of H_2SO_4 , SO_2 , and H_2O at high temperatures. Further study is also necessary to compare and contrast these materials for mixed ionic-electronic conducting membrane applications against a variety of widely published materials' classes known for fast ionic conductivity, mixed electronic-ionic conductivity, high oxygen permeability or a combination of all these characteristics (for example: $\text{La}_{1-x}\text{Sr}_x\text{Co}_{1-y}\text{Fe}_y\text{O}_{3-\delta}$ (LSCF); (La, Sr)(Ga, Mg) O_3). [31]

The $\text{La}_2\text{Ni}_{1-x}\text{M}_x\text{O}_4$ (M = Cu, Zn) phases showed initial promise for S-I membranes due to their thermal cycling stability, relative oxygen uptake ability, and conductivity measurements. Both the substituted and unsubstituted materials had conductivities on the same order of magnitude as the LSCM materials. However, when the La_2NiO_4 phase was made as a pellet and exposed to the conditions inside the H_2SO_4 reactor, it decomposed almost completely. Therefore, no further study is planned with this class of materials as S-I cycle membranes.

ACKNOWLEDGEMENTS

Sandia is a multiprogram laboratory operated by Sandia Corporation, a Lockheed Martin Company, for the US DOE's NNSA, contract DE-AC04-94-A185000. The authors would like to thank our collaborators at Eltron Research, Inc., for on-going permeation experiments, and Dr. Ram Seshadri, Dr. Hongwu Xu and Dr. François Bonhomme for their helpful discussions.

REFERENCES

1. B.C.R. Ewan, R.W.K. Allen *Int. J. Hydrogen Energ.* **30** (2005), p. 809.
2. G.-J. Hwang, K. Onuki *J. Membrane Sci.* **194** (2001), p. 207.
3. S. Goldstein, J.-M. Borgard, X. Vitart *Int. J. Hydrogen Energ.* **30** (2005), p. 619.
4. G.E. Besenbruch, L.C. Brown, J.F. Funk, S.K. Showalter. "High efficiency generation of hydrogen fuels using nuclear power (Proceedings)"; 1st Information Exchange Meeting; October 2-3, 2000; PARIS, FRANCE, 2001, Paris, France.
5. Y. Teraoka, H.M. Zhang, K. Okamoto, N. Yamazoe *Mater. Res. Bull.* **23** (1988), p. 51.
6. Y. Teraoka, T. Nobunaga, K. Okamoto, N. Miura, N. Yamazoe *Solid State Ionics* **48** (1991), p. 207.
7. J.W. Stevenson, T.R. Armstrong, R.D. Carneim, L.R. Pederson, W.J. Weber *J. Electrochem. Soc.* **143** (1996), p. 2722.
8. A. Mineshige, J. Izutsu, M. Nakamura, K. Nigaki, J. Abe, M. Kobune, S. Fujii, T. Yazawa *Solid State Ionics* **176** (2005), p. 1145.
9. H. Kruidhof, H.J.M. Bouwmeester, R.H.E. v. Doorn, A.J. Burggraaf *Solid State Ionics* **63-65** (1993), p. 816.
10. X. Qi, Y. Lin, S. Swartz *Ind. Eng. Chem. Res.* **39** (2000), p. 646.
11. Jade 6.5+; Materials Data Inc.: Livermore, CA, 2002.
12. J. Rodriguez-Carvajal. FullProf.2k; ILL, 2004.
13. F. Gelbard, J. C. Andazola, G. E. Naranjo, C. E. Velasquez, A. R. Reay, "High Pressure Sulfuric Acid Decomposition Experiments for the Sulfur-Iodine Thermochemical Cycle" Sandia National Laboratories, SAND2005-55998, September 2005.
14. A. Petrov, V. Voronin, T. Norby, P. Kofstad *J. Solid State Chem.* **143** (1999), p. 52.
15. Y. Zeng, Y. Lin *Solid State Ion. Diffus. React.* **110** (1998), p. 209.
16. H. Kusaba, G. Sakai, K. Shimanoe, N. Miura, N. Yamazoe *Solid State Ion. Diffus. React.* **152/153** (2002), p. 689.
17. Z. Yang, Y. Lin, Y. Zeng *Ind. Eng. Chem. Res.* **41** (2002), p. 2775.
18. V. Kozhevnikov, I. Leonidov, E. Mitberg, M. Patrakeevev, A. Petrov, K. Poeppelmeier *J. Solid State Chem.* **172** (2003), p. 296.
19. M. Axness, "Synthesis and Characterization of Metal Oxides", Sandia National Laboratories Summer Intern Program (SIP), final report and presentation, July 2005.
20. Shannon, *Acta Cryst.* **A32** (1972), 751.
21. Bezdiccka et al., *Z. fur. Anorgan. Allege. Chemie* **619** (1993), p. 7
22. Matar et al., *J. Mater. Chem.* **6** (1996), p. 1785
23. Ishikawa et al., *Phys. Rev. Lett.* **93** (2004), p. 136401.
24. Korotin et al., *Phys. Rev. B* **54** (1996), p. 5309.
25. Imada et al., *Rev. Mod. Phys.* **70** (1998), p.1039.
26. Sarm et al., *Phys. Rev. Lett.* **75** (1995), p.1126.
27. Singh et al., *Phys. Rev. B* **43** (1991), p. 11628.
28. Leung, *Phys. Rev. B* **63** (2001), p. 134415.
29. Mackay, R., "Oxygen Permeation Data", Final Report for Contract No. PO547525 prepared for Andrea Ambrosini, March 9, 2006.

30. Ambrosini, A.; Garino, T.; Nenoff, T. M. "Synthesis and Characterization of the double-substituted perovskites $\text{La}_x\text{Sr}_{1-x}\text{Co}_{1-y}\text{Mn}_y\text{O}_{3-d}$ for use in high temperature oxygen separations", *Solid State Ionics*, **2006**, 177, 2275-2279.
31. (a) X. Qi, Y. S. Lin, S. L. Swartz, *Ind. Eng. Chem. Res.* **39** (2000), p. 646 and references within; (b) M. Matsuda, O. Ohara, K. Murata, S. Ohara, T. Fukui, M. Miyake, *Electrochemical and Solid State Letters* **6** (2003), p. A140.; (c) J. C. Boivin, G. Mairesse, "Recent Developments in Fast Oxide Ion Conductors" *Chem. Mater.* **10** (1998) 2870.

FIGURE CAPTIONS

Fig. 1: Rietveld refinements of the powder X-ray diffraction pattern for $\text{La}_{0.1}\text{Sr}_{0.9}\text{Co}_{0.7}\text{Mn}_{0.3}\text{O}_{3-\delta}$. Space group = $Pm-3m$ (221).

Fig. 2: PXRD patterns of $\text{La}_{0.1}\text{Sr}_{0.9}\text{Co}_y\text{Mn}_{1-y}\text{O}_{3-\delta}$ ($0.1 \leq y \leq 0.5$).

Fig. 3: Multiple cycle TGA (temperature and %weight loss vs. time) of (a) $\text{La}_{0.1}\text{Sr}_{0.9}\text{Co}_{0.7}\text{Mn}_{0.3}\text{O}_{3-\delta}$ and (b) Y:ZrO₂ (3%).

Fig. 4: Conductivity vs. (a) temperature in air and (b) pO₂ at 900 °C for LSCM1991, LSCM 1973, and YSZ (3%).

Fig. 5: Conductivity vs. temperature in air for $\text{La}_2\text{Ni}_{1-x}\text{M}_x\text{O}_4$ samples.

Fig. 6: Three plots of the enthalpies of formation versus oxygen content, total cobalt content and average oxidation state of Mn

Fig. 7: XRD of LSCM1973 pellet, (a) as-sintered, (b) ground up after exposure in H₂SO₄, and (c) surface of pellet after exposure in reactor.

Fig. 8: SEM of surface of LSCM membrane (left) before and (right) after exposure in H₂SO₄.

Fig. 9: Top: SEM of (left) cross-section with (right) EDS map area magnified; **Bottom:** EDS maps of Sr, Co, and S.

Fig. 10: Permeation and activation energy for LSCM phases, tested at Eltron Research, Inc. [29]

Table 1a: Composition, phase purity, cubic lattice parameter, and average weight loss from TGA for members of the family $\text{La}_x\text{Sr}_{1-x}\text{Co}_y\text{Mn}_{1-y}\text{O}_{3-\delta}$ (LSCM).

Nominal Composition	Single Phase?	Lattice parameter, a (Å)*	Avg. Weight Loss vs. T	Avg. Weight Loss vs. Atm
$\text{La}_{0.1}\text{Sr}_{0.9}\text{Co}_{0.9}\text{Mn}_{0.1}\text{O}_{3-\delta}$ (LSCM1991)	Yes	3.845	1.36%	0.707%
$\text{La}_{0.1}\text{Sr}_{0.9}\text{Co}_{0.8}\text{Mn}_{0.2}\text{O}_{3-\delta}$ (LSCM1982)	Yes	3.844	1.13%	0.780%
$\text{La}_{0.1}\text{Sr}_{0.9}\text{Co}_{0.7}\text{Mn}_{0.3}\text{O}_{3-\delta}$ (LSCM1973)	Yes	3.841	0.949%	0.910%
$\text{La}_{0.1}\text{Sr}_{0.9}\text{Co}_{0.6}\text{Mn}_{0.4}\text{O}_{3-\delta}$ (LSCM1964)	No	3.835	0.766%	0.725%
$\text{La}_{0.1}\text{Sr}_{0.9}\text{Co}_{0.5}\text{Mn}_{0.5}\text{O}_{3-\delta}$ (LSCM1955)	No	3.835	0.458%	0.573%
$\text{La}_{0.1}\text{Sr}_{0.9}\text{Co}_{0.3}\text{Mn}_{0.7}\text{O}_{3-\delta}$ (LSCM1937)	No	3.820	N/A	N/A
$\text{La}_{0.2}\text{Sr}_{0.8}\text{Co}_{0.9}\text{Mn}_{0.1}\text{O}_{3-\delta}$ (LSCM2891)	No	3.836	1.414%	0.458
$\text{La}_{0.2}\text{Sr}_{0.8}\text{Co}_{0.6}\text{Mn}_{0.4}\text{O}_{3-\delta}$ (LSCM2864)	Yes	3.834	0.850%	0.509%
$\text{La}_{0.5}\text{Sr}_{0.5}\text{Co}_{0.5}\text{Mn}_{0.5}\text{O}_{3-\delta}$ (LSCM5555)	Yes	3.848	0.1873%	0.1774%
$\text{La}_{0.1}\text{Sr}_{0.9}\text{Co}_{0.9}\text{Fe}_{0.1}\text{O}_{3-\delta}$ (LSCF1991)	Yes			
$\text{La}_{0.1}\text{Sr}_{0.9}\text{CoO}_{3-\delta}$ (LSC)	Yes			
Y:ZrO ₂ (3%)	Yes	---	0.470%	0.0955%

* Lattice parameter of predominant perovskite phase indexed in the $Pm-3m$ space group, calculated using the JADE peak fit program.

Table 1b: Composition, phase purity, cubic lattice parameter, and average weight loss from TGA for members of the family $\text{La}_2\text{Ni}_{1-x}\text{M}_x\text{O}_4$ (M. Axness, SIP final report FY05)

Nominal Composition	Single Phase?	Avg. Weight Loss vs. T	Avg. Weight Loss vs. pO ₂
La_2NiO_4	Y	0.262 %	0.0710 %
$\text{La}_2\text{Ni}_{0.8}\text{Zn}_{0.2}\text{O}_4$	Y	0.266 %	0.125 %
$\text{La}_2\text{Ni}_{0.6}\text{Zn}_{0.4}\text{O}_4$	Y	0.201 %	0.178 %
$\text{La}_2\text{Ni}_{0.4}\text{Zn}_{0.6}\text{O}_4$	N	0.241 %	0.130 %
$\text{La}_2\text{Ni}_{0.8}\text{Cu}_{0.2}\text{O}_4$	Y	0.255 %	0.095 %
$\text{La}_2\text{Ni}_{0.6}\text{Cu}_{0.4}\text{O}_4$	Y	0.261 %	0.119 %
$\text{La}_2\text{Ni}_{0.4}\text{Cu}_{0.6}\text{O}_4$	Y	0.238 %	0.083 %

Figure 1

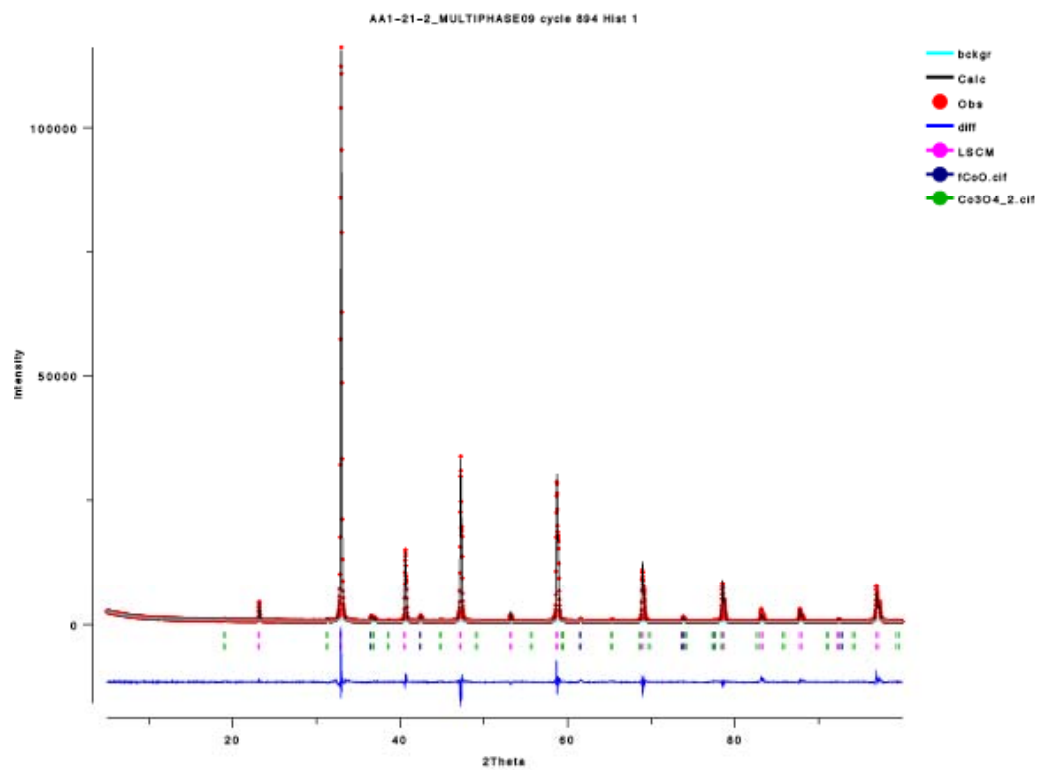


Figure 2

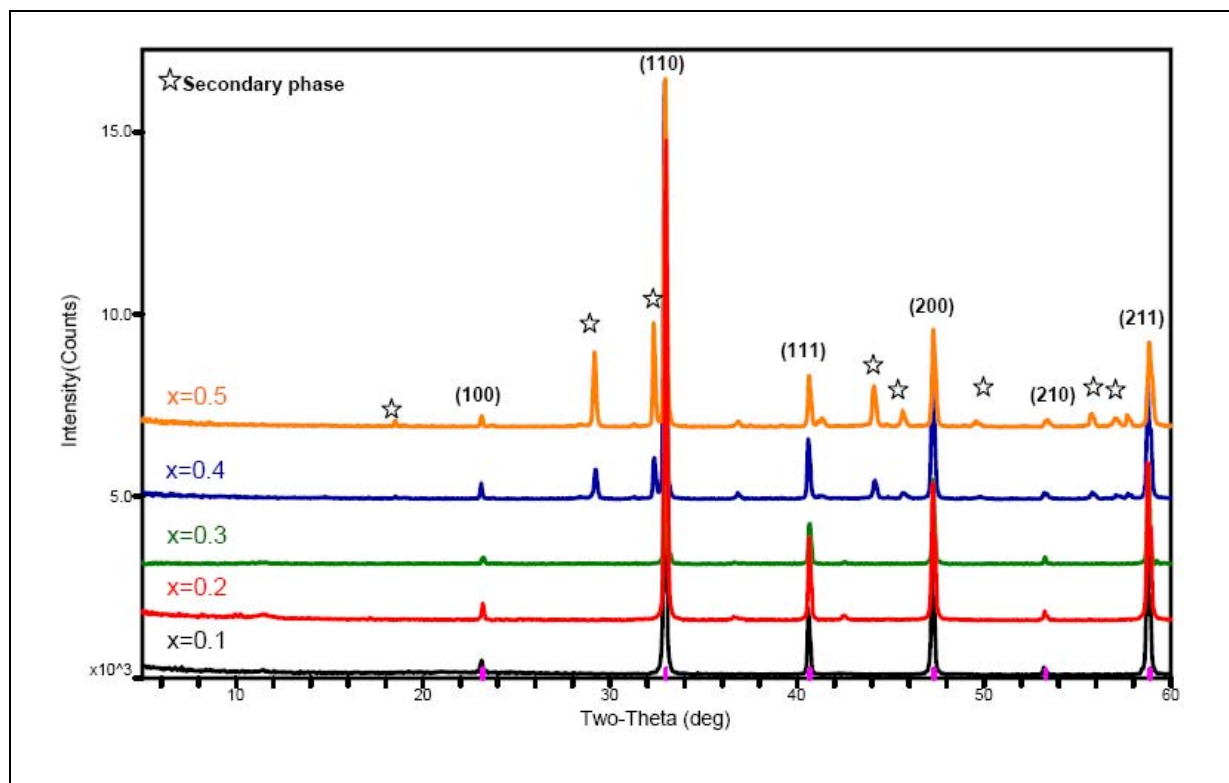


Figure 3 (a-b)

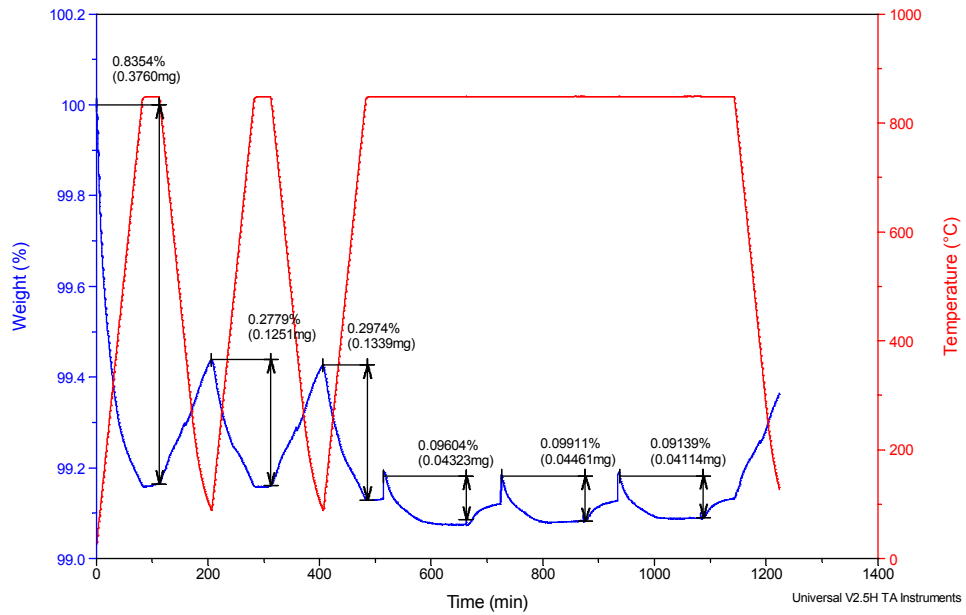
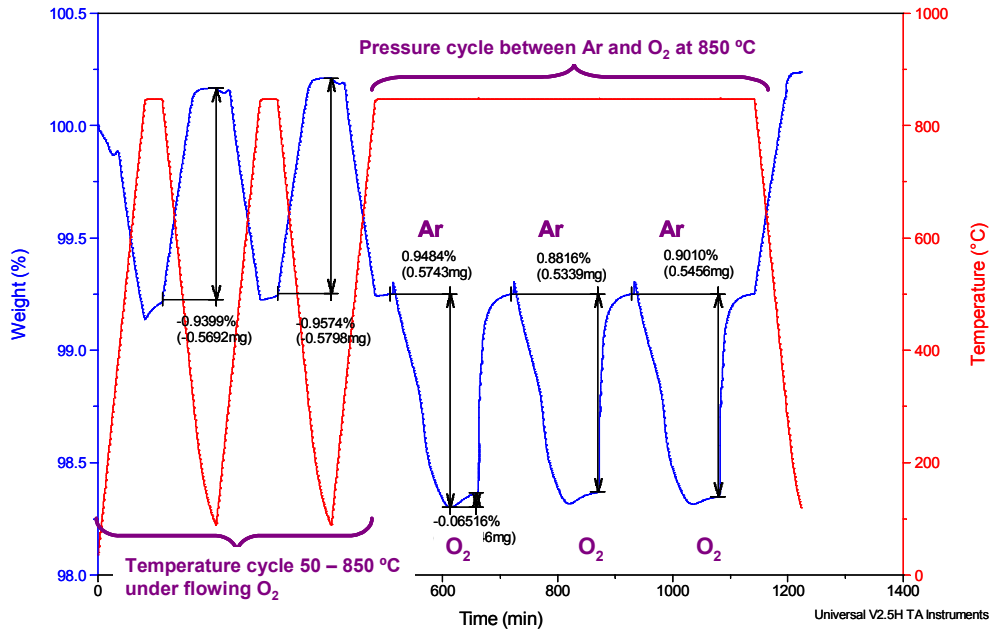


Figure 4.

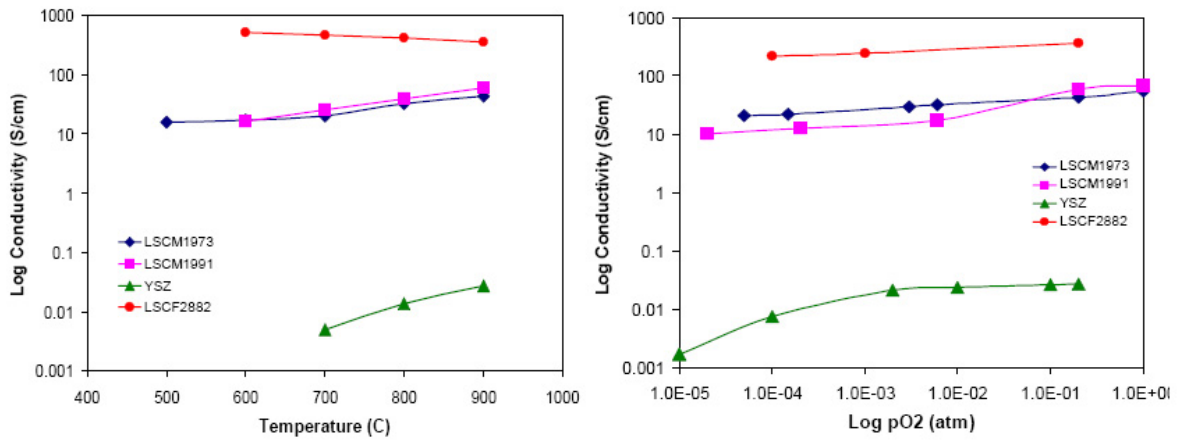


Figure 5.

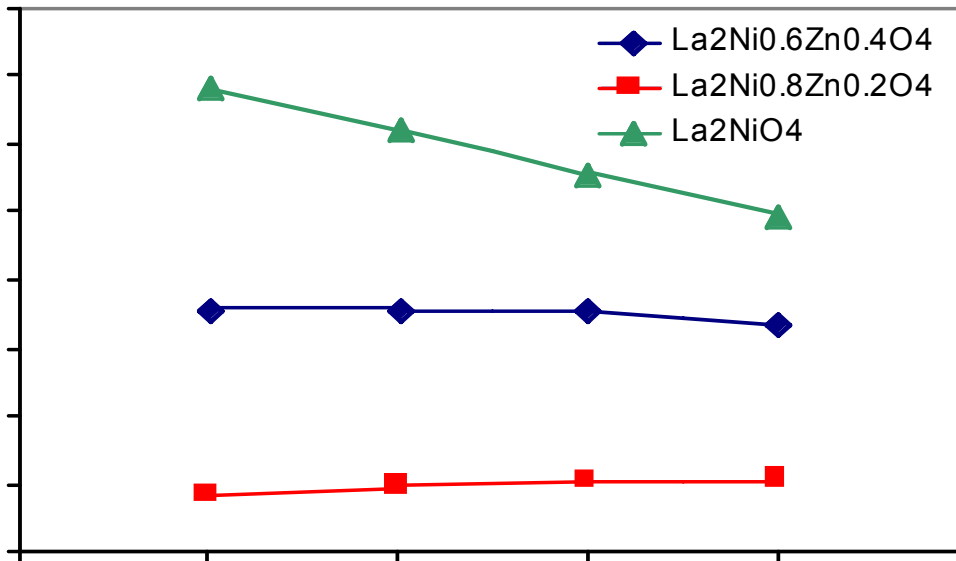
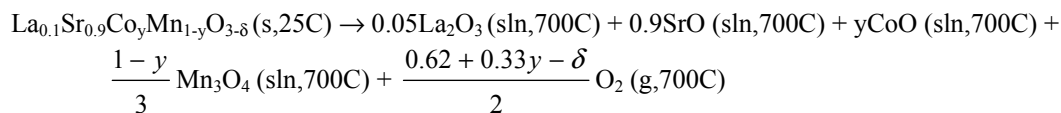
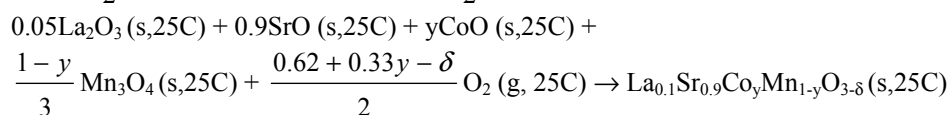
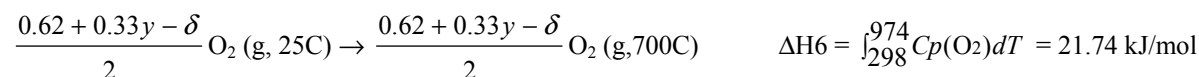
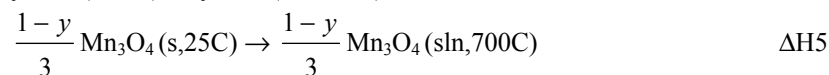
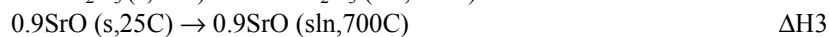
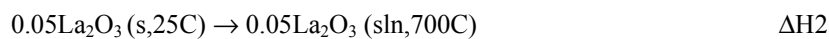
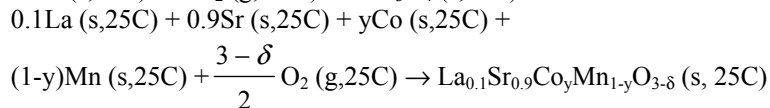
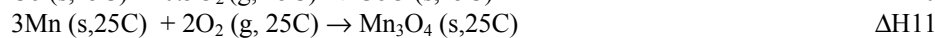
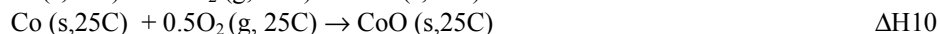
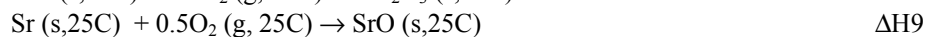
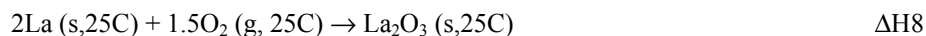


Table 2: Enthalpy of formation of $\text{La}_{0.1}\text{Sr}_{0.9}\text{Co}_y\text{Mn}_{1-y}\text{O}_{3-\delta}$ from oxides and elements

$$\Delta\text{H1} = \Delta\text{H}_{\text{ds}}$$



$$\Delta\text{H7} = \Delta\text{H}_{\text{ox}}^0 = 0.05\Delta\text{H2} + 0.9\Delta\text{H3} + y\Delta\text{H4} + \frac{1-y}{3}\Delta\text{H5} + \frac{0.62+0.33y-\delta}{2}\Delta\text{H6} - \Delta\text{H1}$$



$$\Delta\text{H12} = \Delta\text{H}_{\text{el}}^0 = 0.05\Delta\text{H8} + 0.9\Delta\text{H9} + y\Delta\text{H10} + \frac{1-y}{3}\Delta\text{H11} + \Delta\text{H7}$$

Compound	$\Delta\text{H}_{\text{ds}}$ kJ/mol	$\Delta\text{H}_{\text{ox}}^0$ kJ/mol	$\Delta\text{H}_{\text{el}}^0$ kJ/mol
$\text{La}_{0.1}\text{Sr}_{0.9}\text{Co}_{0.9}\text{Mn}_{0.1}\text{O}_{2.76}$	6.86 ± 0.17 (8)	-113.52 ± 2.28	-994.81 ± 2.7
$\text{La}_{0.1}\text{Sr}_{0.9}\text{Co}_{0.8}\text{Mn}_{0.2}\text{O}_{2.76}$	2.57 ± 0.18 (6)	-105.43 ± 2.27	-1009.08 ± 2.63
$\text{La}_{0.1}\text{Sr}_{0.9}\text{Co}_{0.65}\text{Mn}_{0.35}\text{O}_{2.8}$	18.89 ± 0.31 (8)	-115.60 ± 2.28	-1052.80 ± 2.59
La_2O_3	-225 ± 3.16		-1791.6 ± 2.0
SrO	-135.82 ± 2.48		-590.5 ± 0.9
CoO	15.35 ± 0.45		-237.9 ± 1.3
Mn_3O_4	170.6 ± 1.0		-1384.5

Figure 6 (a-c).

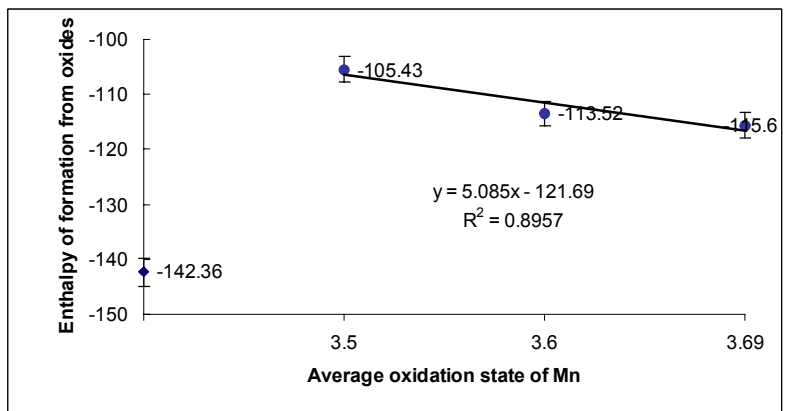
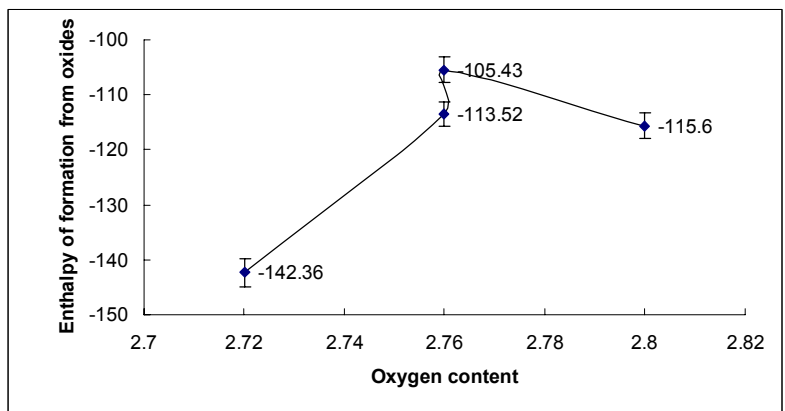
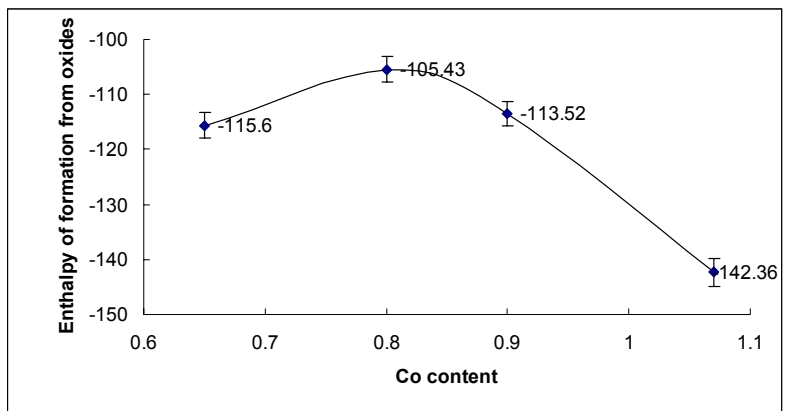


Figure 7.

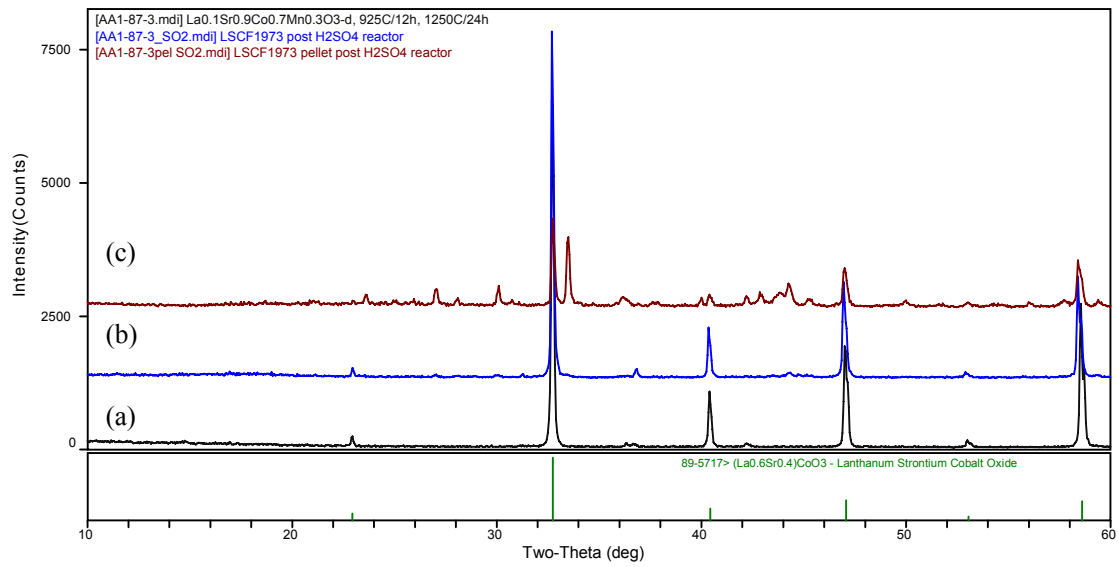


Figure 8.

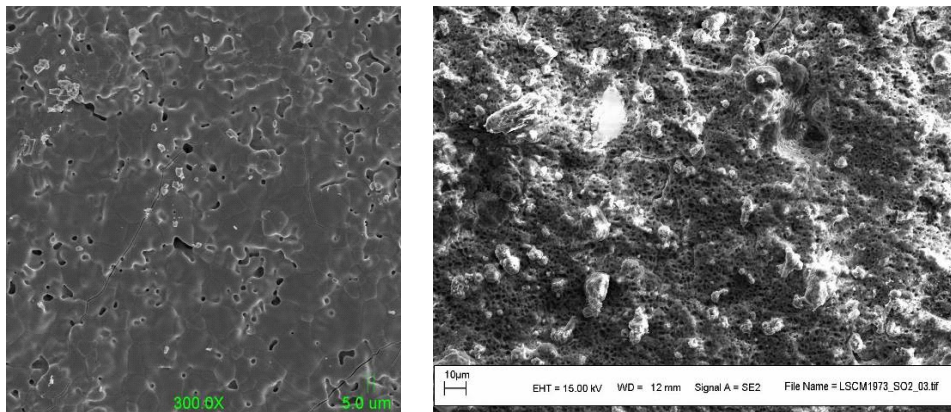


Figure 9.

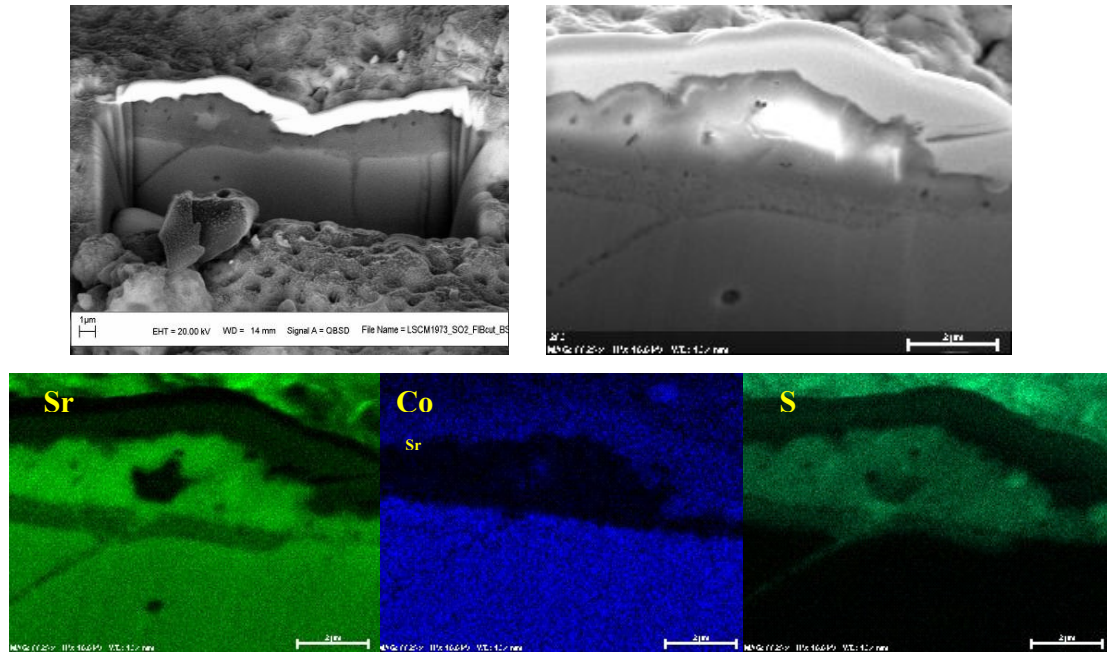
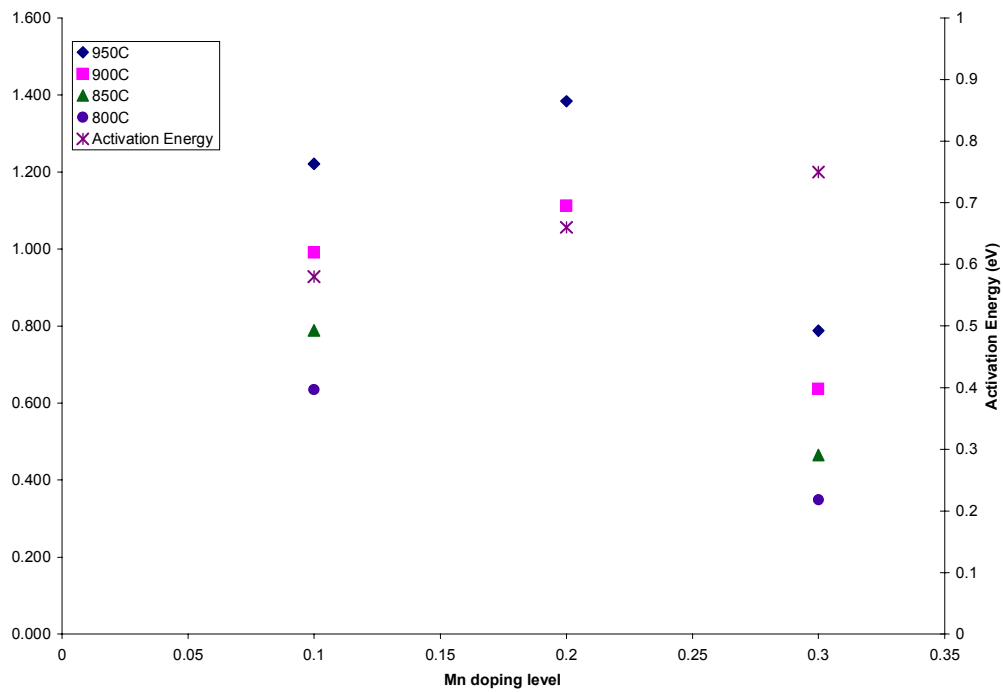


Figure 10.



Distribution List

5	MS1415	Tina M. Nenoff, 1114
5	MS0734	Andrea Ambrosini, 6338
1	MS1411	Terry Garino, 1816
1	MS1415	Kevin Leung, 1114
1	MS1136	Fred Gelbard, 6771
1	MS1415	Carlos Gutierrez, 1114
1	MS1415	James Voigt, 1816
1	MS0734	J. Bruce Kelley, 6334
1	MS1136	Paul Pickard, 6771
1	MS0734	Ellen Stechel, 6338
1	MS0779	Carl Axness, 6772
2	MS9018	Central Technical Files, 8944
2	MS0899	Technical Library, 4536

1 Dr. Harold Wright, VP – Technology
Eltron Research Inc.
4600 Nautilus Court South
Boulder, CO 80301-3241

2 Dr. Richard Mackay, Ceramic Technology Manager
Eltron Research Inc.
4600 Nautilus Court South
Boulder, CO 80301-3241

2 Dr. Alexandra Navrotsky
Thermochemistry Facility and NEAT ORU
University of California at Davis
One Shields Avenue
Davis, CA 95616-8779